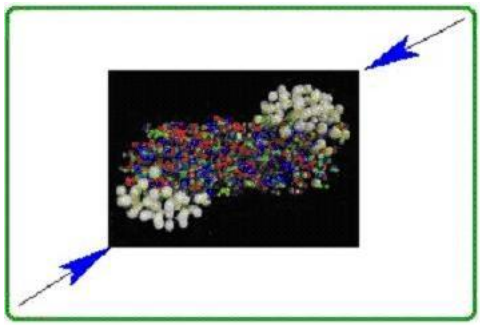

High Energy

High Intensity

Hadron Beams

Simulation of "Crystal", the bent crystal based collimation experiment in the SPS

W. Scandale, A. Taratin

CERN, CH-1211 Geneva 23, Switzerland

Abstract

Crystal collimation is a possible variant of the two-stage collimation systems used in modern accelerators, by which the collimation efficiency may be strongly enhanced. An experiment is proposed in the CERN-SPS to check the improved performance on crystal collimation. Here we present the experiment layout and we perform simulations showing in quantitative manner the expected behavior of crystal collimation in the SPS.

EU contract number RII3-CT-2003-506395 CARE-Note-2008-007-HHH

EUROPEAN ORGANIZATION FOR NUCLEAR RESEARCH
Laboratory for Particle Physics

Departmental Report **CERN/AT 2008-21**

SIMULATION OF "CRYSTAL", THE BENT CRYSTAL BASED COLLIMATION EXPERIMENT IN THE SPS

W. Scandale and A. Taratin
CERN, Geneva, Switzerland

Crystal collimation is a possible variant of the two-stage collimation systems used in modern accelerators, by which the collimation efficiency may be strongly enhanced. An experiment is proposed in the CERN-SPS to check the improved performance on crystal collimation. Here we present the experiment layout and we perform simulations showing in quantitative manner the expected behavior of crystal collimation in the SPS.

CERN-AT-2008-021
26/08/2008

CERN
Accelerator Technology Department
CH - 1211 Geneva 23
Switzerland

26 August 2008

1. Introduction

In high intensity modern accelerators, high performing collimation systems are required. They generally rely on a two-stage layout, in which the primary scraper eventually deflects the halo particles through multiple scattering onto the secondary bulk absorber.

CRYSTAL is an experiment to be performed in the SPS in the following years [1], with the aim of testing if bent crystals, used as primary collimators in a two-stage collimation system, are more effective that amorphous collimators. The underlying idea is that, for given angular orientations, due to channeling or volume reflection [2], the crystal should induce a preferential deflection in the trajectories of the primary halo and hence a larger impact parameter and angle into the secondary absorber.

Figure 1 shows the layout of CRYSTAL in the long straight section 5 of the SPS. The bent crystal, located upstream of the focusing quadrupole QF518, intercept the incoming particles and eventually deflect them in the horizontal plane, towards outside the SPS circle, onto the secondary tungsten absorber 60 cm long (TAL), installed upstream of the focusing quadrupole QF520. Two roman pots, located between the defocusing quadrupole DQ519 and the TAL, contain silicon strip detectors, which should provide information on the deflected beam trajectories, on the incoming flux and on the collimation efficiency.

In this note we present results of computer simulations to estimate if the above layout is appropriate for collimation and to evaluate the collimation efficiency when the circulating particles are deliberately perturbed in order to produce a diffusive growth of their emittance. The primary collimator is assumed to be a single crystal. Multi-crystal systems will be considered at a later stage.

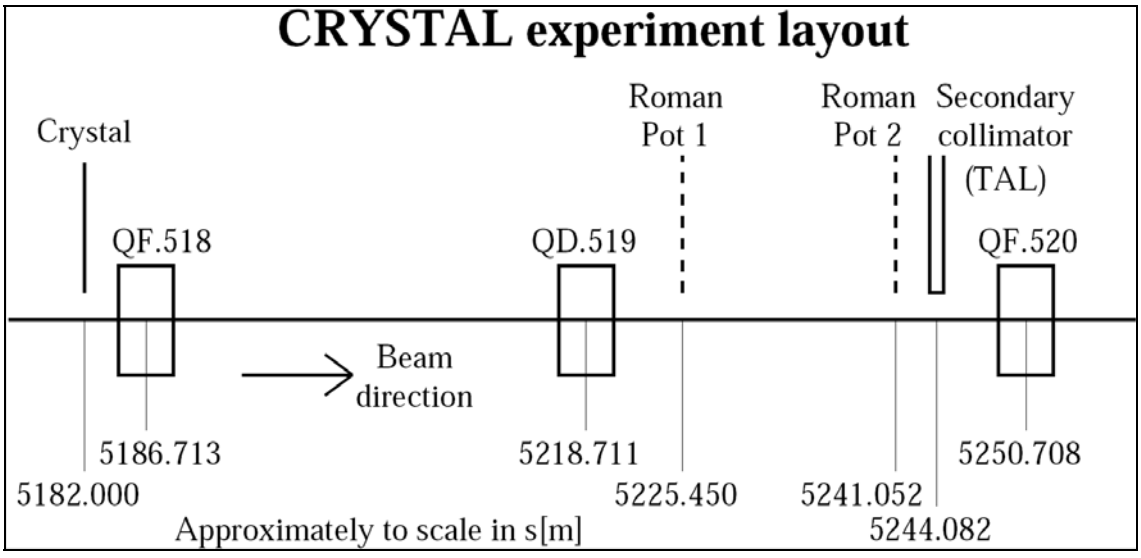

Figure 1: Schematic layout of the CRYSTAL experiment in the SPS.

2. Beam and crystal parameters

We selected two energies of interest to perform collimation experiments with CRYSTAL, 120 and 270 GeV. The first value of 120 GeV is the energy of the RD22 [3], a crystal extraction experiment performed in the early nineties in the SPS, for which we have numerous reference data in the literature. The second value of 270 GeV is the energy of other machine experiments planned in the SPS simultaneously to CRYSTAL, a choice that may significantly speed-up the required setting-up of the accelerator during the test periods.

The beam parameters will be those of Table 1, where the transverse RMS beam radius is computed in the middle of a focusing quadrupole, whilst the tunes are the ones for the high intensity operation mode of the SPS. The beam intensity will be of a few 10^{11} up to a few10^{12} particles. The RF beam structure will be either unbunched or bunched in a few tens of bunches. The accelerator will operate in storage mode.

Table 1: SPS beam parameters

	High energy	**Unbunched**	**Bunched**
Momentum P [GeV/c]	270	120	120
Tune Qx	26.13	26.13	26.13
Tune Qy	26.18	26.18	26.18
Tune Qs	0.0021	0	0.004
Normalized emittance (at 1 σ) [mm mrad]	1.5	1.5	1.5
Transverse radius (RMS) [mm]	0.67	1	1
Momentum spread (RMS) Δp/p	2 to 3×10^{-4}	2 to 3×10^{-4}	4×10^{-4}
Longitudinal emittance [eV-s]	0.4	≤0.4	0.4
RF Voltage [MV]	1.5	0	1.5

The beam lifetime is determined by the SPS vacuum and should be larger than 80 h. By applying an external noise we should be able to reduce the beam lifetime to a value ranging from a few tenths of minutes to a tenth of hour. A similar approach had been used successfully in RD22, with the hardware still currently operational in the SPS. The subsequent halo flux hitting the crystal should be sustainable by our detectors in the roman pots. In practice, we will produce one of the following conditions:

- A halo flux in the range of a few 10^2 to a few 10^4 particles per turn "equally" distributed along the revolution period (unbunched beam); or synchronous to the bunch structure (bunched beam), which can be investigated with the detectors in the roman pots, avoiding counting saturation.
- Larger fluxes up to a few 10^5 particles per turn, which may saturate the monitors in the roman pots and hence should be studied using only the beam loss monitors of the SPS.

The primary collimator is a silicon crystal 0.5 mm thick, oriented along the (111) planes, with a bend angle α=150 μrad and a length along the beam L=1 mm. This gives a bend radius R=6.67 m (the critical radius for 120 GeV protons is R_c=21.46 cm). In these conditions, the particles deflected in the TAL should have large impact parameters, of about 6-8 mm.

The crystal bend radius, which produces the maximum extraction efficiency for 120 GeV protons, is about 1-2 m, i.e. about 5-10 times R_c. The crystal parameters, α and L, we selected are a sound compromise in between the optimal values for SPS and those eventually required for LHC. The selected crystal parameters are easy to be achieved with both anticlastic and quasi-mosaic bending techniques.

3. Experimental layout of CRYSTAL

The layout of CRYSTAL is shown in Figure 1. We selected it on the basis of simple arguments. We decided to deflect the halo particles in the horizontal plane where the SPS aperture is larger. All the components of CRYSTAL are retractable to allow an easy routine operation at high intensity, whenever required. The layout is as compact as possible to save on cost of cables. Two roman pots RP1 and RP2 equipped with silicon strips are used to detect the particles deflected towards the TAL and to measure their coordinate and angle. For cost

saving, we will reuse the TOTEM prototype roman pot, already tested in the SPS, and we will build a new roman pot of the same design [4]. The existing roman pot has a round aperture of 80 mm, imposing us to install it close to a defocusing quadrupole where the horizontal beam size is small enough. The new roman pot will have a round aperture of 160 mm and can be installed anywere in the SPS lattice.

In collimation mode, the clearance of the deflected particles from the circulating beam should be large enough, i.e. at least of some millimeters, for two reasons. We want to detect a clear signal of the deflected beam and intercept it with high efficiency, avoiding tight tolerance on the mechanical flatness and on the lateral positionning of roman pots and TAL. At the same time, we want to measure the residual particle density in a large fraction of the clearance area and check to which extent it is really empty, as in fact we suppose it should be.

For a rough estimate of the beam clearance we used qualitative considerations.

In normalized coordinates [4], an angular deflection θ applied to a particle circulating along the closed orbit, in a location where $\beta=\beta_d$, produces at an observation point where $\beta=\beta_o$ the orbit perturbation

$$\Delta x = \theta \cdot (\beta_d \cdot \beta_o)^{\frac{1}{2}} \cdot \sin \Delta\psi ,$$

where $\Delta\psi$ is the betatron phase advance between the observation and the deflection point.

The deflection has the maximal effect when β_d is close to β_{max}, whilst the deviation is maximal in the locations where β is close to β_{max} and $\Delta\psi$ close to an odd multiple of 0.25. In the SPS, it is easy to fill these requirements, by choosing the deflection and the observation points close to QF quadrupoles, one cell apart. This will imply $\beta_d \approx \beta_o \approx \beta_{max}$, and $\Delta\psi \approx 0.25$.

In fact, the crystal should intercept halo particles and not particles circulating along the closed orbit. For this reason it will be located at the distance x_{bc} from the beam centre, thereby inducing in the deflected particles the phase shift

$$\Delta\varphi = \arccos[(1+(\beta_{bc}\theta / x_{bc})^2)^{-1/2}], \quad \Delta\psi = \frac{\Delta\varphi}{2\pi}.$$

The optimal phase advance from the deflection to the observation points is accordingly reduced and it will be no longer possible to find positions in the SPS simultaneously matching the optimal conditions for β and $\Delta\psi$.

In operational conditions, the crystal will be typically shifted by 6 times the RMS beam size σ_{beam} from the closed orbit. With the transverse emittance of Table 1, this imply $x_{bc}=6\cdot\sigma_{beam}=6.345$ mm. For $\alpha=150$ μrad, the angular kick due to channelling will be $\theta=\alpha$. The subsequent betatron phase shift of the deflected particles will be $\Delta\varphi=1.156$ rad, which imply $\Delta\psi=0.184$.

The previous considerations guided us in choosing the experimental layout of Figure 1. The crystal will be located in the free space at S=5182 m, upstream of QF518, and the TAL in the free space at S=5244.082 m, upstream QF520. The new roman pot, called RP2, will be placed near to the TAL, in the free space at S=5241.05 m, where a larger aperture is required. The old roman pot, called RP1, will be placed upstream of RP2 at a sufficient distance to allow detecting with large accuracy the angle of the deflected trajectories. Due also to its reduced aperture, RP1 will be placed in the free space at S=5225.45 m, close to the defocusing quadruple QD519, where the horizontal beam size is small. In these conditions, a 10 μm resolution in the silicon strips should allow angular resolutions of 10^{-3} mrad.

The values of the betatron functions in the locations of interest are given in Table 2. The crystal, the TAL and RP2 are all close to β_{max} locations, but the phase advance from the TAL

and RP2 to the crystal is too large respect to the above optimal value. Instead, in the RP1 location the β-value is small and the phase advance optimal. In all cases, the clearance should be larger than a few mm at the two roman pots and at the TAL locations.

A precise estimate of the beam deviation will result from computer simulations, in which all the lattice parameters will be accounted in full detail. The results of these simulations performed at 120 GeV will be discussed hereafter. Simulations at 270 GeV will be performed at a later stage.

Table 2: betatronic functions of the CRYSTAL components in the SPS

Name	S [m]	β_x [m]	$\Delta\psi_x$ [rad]	D_x [m]	β_y [m]	$\Delta\psi_y$ [rad]
Crystal	5182	96.048	0	-0.880	22.687	0
QF518	5186.7129	103.429	0.0072	-0.909	20.781	0.0362
QD519	5218.7106	20.969	0.1379	-0.244	103.351	0.1481
RP1	5225.45	31.004	0.1804	-0.179	75.041	0.1602
RP2	5243.45	85.180	0.2374	-0.006	26.659	0.2262
TAL	5245.125	92.247	0.2404	0.010	24.171	0.2367
Q520	5250.7083	103.424	0.2491	0.060	21.106	0.2782

4. Transverse positions of the CRYSTAL devises

As already mentioned, in operational conditions, the bent crystal will act as the primary halo collimator and its edge will be at the distance of $x_{bc}=6\sigma_{beam}$ from the closed orbit. Also the TAL and of the two roman pots will be retracted from the beam centre, at a distance which must be larger than that choosen for the crystal. By this choice, we want to guarantee in all circumstances that the crystal will intercept the halo particles before any other experimental devise, thereby acting as the effective primary collimator. We also want to ensure that halo particles, which are not channeled in the first crystal passage and which are deflected by multiple scattering as if the crystal was an amorphous material, can hit the crystal again in the subsequent revolutions, thereby having additional chances of being eventually channeled. In other word, we want that during our test the multi-turn channeling mechanism, discovered in RD22 [2], is fully active and can eventually produce the maximal collimation efficiency.

The simplest option is to position the edges of the two roman pots and of the TAL, in normalized coordinates, at the same distance $6\sigma_{beam}+x_{of}$ from the beam centre, shifted by the same offset x_{of} respect to the crystal edge position. The size of x_{of} is choosen in shuch way that the multi-turn effect has a high probability of happening. Non-channeled 120 GeV particles, in traversing the 1 mm long Silicon crystal, are randomly scattered in all directions. The RMS scattering angle is $\theta_{ms}\approx 10$ μrad. We require that particles deflected by up to $4.25\cdot\theta_{ms}$ in the horizontal plane stay clear from the TAL and the roman pots. By this choice, the probability of loosing multiple scattered particles in the first turn becomes negligible, i.e. of the order of 10^{-5}.

In Table 3 we give the nominal values of the beam edge at $6\sigma_{beam}$, of the offset x_{of} and of distance $6\sigma_{beam}+x_{of}$ from the beam centre at the location of the CRYSTAL devises.

Table 3: Beam size and distances of the CRYSTAL devises from the beam centre

	Crystal	**QD519**	**RP1**	**RP2**	**TAL**	**QF520**
$6\sigma_{beam}$ [mm]	6.35	2.97	3.61	5.98	6.23	6.60
x_{of} [mm]	0	0.41	0.5	0.83	0.86	0.91
$6\sigma_{beam}+x_{of}$ [mm]	6.35	3.38	4.11	6.81	7.09	7.31

5. Roman pot model for simulations

The roman pots, schematically shown in Figure 2, are vacuum tight metallic boxes, which can be inserted in the vacuum pipe to bring silicon strip detectors close to the circulating beam. Each metallic box has a 3×4 cm^2 cross section with 200 μm thick transversal windows in stainless steel and a 150 μm thick longitudinal window in aluminium. The detecting planes are three in RP1 and five in RP2. Each of them, 300 μm thick, has a 2×3 cm^2 sensitive section, ending by a 500 μm wide insensitive area towards the beam side. When inserted in the roman pot, each strip has a 150 μm clearance from the longitudinal window. In the box there is a secondary vacuum with a 10^{-6} tor residual pressure.

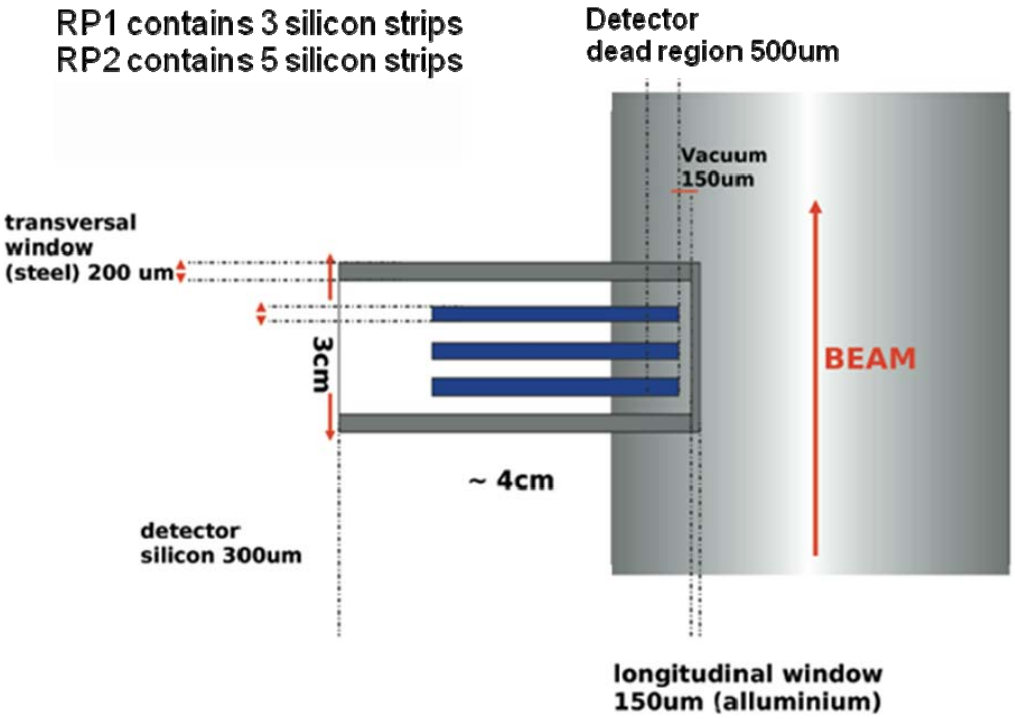

Figure 2: Schematic description of the roman pot and the silicon detectors.

Particles of increasing betatron amplitude, in traversing the pot, see three regions where they interact with different materials. The first area, t_b=150 μm wide, is the aluminum button with an interaction length L_b=3 cm(Al). The second area, t_s=150 μm wide, is the clearance slot with L_s=400 μm(Fe). The third area is the detector area with an interaction length L_d(RP1)=400 μm (Fe)+900 μm (Si) in RP1 and L_d(RP2)=400 μm (Fe)+1500 μm (Si) in RP2 respectively. The insensitive area is t_d=500 μm wide, hence the edge of the sensitive detector area starts at the distance t_{nr}=800 μm from the inner edge of the metallic box. Nuclear interactions and the ionization energy losses are computed in simulating the pot traversal.

With the configuration of Table 2, some particles, lost at the edge of the TAL, may be invisible since they will cross the dead area of the detectors. To minimize their number, the offset and the transverse position of the TAL will be respectively increased to

$$\tilde{x}_{of}(TAL) = x_{of}(TAL) + t_{nr} = 1.66\ mm \quad \Rightarrow \quad 6\sigma_{beam} + \tilde{x}_{of}(TAL) = 8.75\ mm$$

6. Initial distribution of the beam halo particles

As already mentioned in Section 2, the external noise applied to the SPS horizontal damper will produce a continuous emittance growth and a diffusive halo surrounding the circulating beam, resulting in a continuous flux of protons eventually hitting the bent crystal.

We want to describe the initial distribution of the particle coordinates at the first crystal hit, using a simplified argorithm easy to implement in computer simulations. At the crystal azimuth, the normalized betatron amplitude will be written as $x_m=x_{bc}+\Delta x_m$, where x_{bc} is the coordinate of the crystal edge and Δx_m is a random value determined by the exponenitial probability low $P(\Delta x_m)$. Assuming that λ=0.1 μm is the most likely value of Δx_m, we have

$$P(\Delta x_m) = \exp(-\Delta x_m / \lambda)\,, \quad \lambda = 0.1\ \mu m\,, \quad \Delta x_m = -\lambda \ln \xi_1\,,$$

where ξ_1 is a random number choosen with uniform probability in the interval (0,1). The betatron phase advance φ will be written as a random value in the interval ($-\Delta\varphi,\Delta\varphi$), with

$$\Delta\varphi = \arccos(1/(1+\Delta x_m / x_{bc}))\,.$$

The value of φ will be

$$\varphi(\xi_2) = 2\Delta\varphi(\xi_2 - 0.5)\,,$$

where ξ_2 is also choosen with uniform probability in the interval (0,1). In real coordinates, the amplitude and phase of a particle at the first crystal hit will be written as

$$x(\xi_1,\xi_2) = x_m(\xi_1)\cos(\varphi(\xi_2))\,,$$

$$x'(\xi_1,\xi_2) = -\frac{x_m(\xi_1)}{\beta_x}\left[\sin(\varphi(\xi_2)) + \alpha_x \cos(\varphi(\xi_2))\right],$$

where β_x=96.048 m and α_x=-2.216 are the betatronic functions at the crystal azimuth.

For the vertical phase coordinates (y,y') and momentum deviation $\delta=\Delta p/p_o$ we will assume point like distributions centred around zero, i.e. P(y)=P(y')=P(δ)=δ(0).

7. Simulation scenario

In performing particle tracking, we consider the SPS as a linear machine without sextupoles, no momentum spread and no aperture restrictions, except than in the crystal collimation area.

The transverse positions of the collimation devises, discussed in previous Sections 4 and 5, are sketched in Figure 3. The position of the bent crystal determines the $6\sigma_{beam}$ size of the beam envelope. The positions of RP1 and RP2 fix the clearance of the particles deflected by multiple scattering in the crystal, which correspond to a deflecting angle of $4.25\theta_{ms}$=42.5μrad. The TAL position is even more retracted respect to the clearance line in order to increase the fraction of particles, which intercept the sensitive part of the detectors before being absorbed in the TAL.

To speed-up simulations, in each revolution, we transport particles along the four SPS azimuths where the bent crystal BC, the RP1, the RP2 and the TAL are located, using four lumped transfer matrices M(6,6).

The trajectory of each halo particle starts at the crystal azimuth, with initial coordinates extracted from the random distribution decribed in Section 6 and ends either when the particle is absorbed by the TAL or when it has an inelastic interaction in the crystal or in the roman

pots. Nuclear interactions with the detector and roman pot material produce non-localized losses, thereby reducing the collimation efficiency of the TAL.

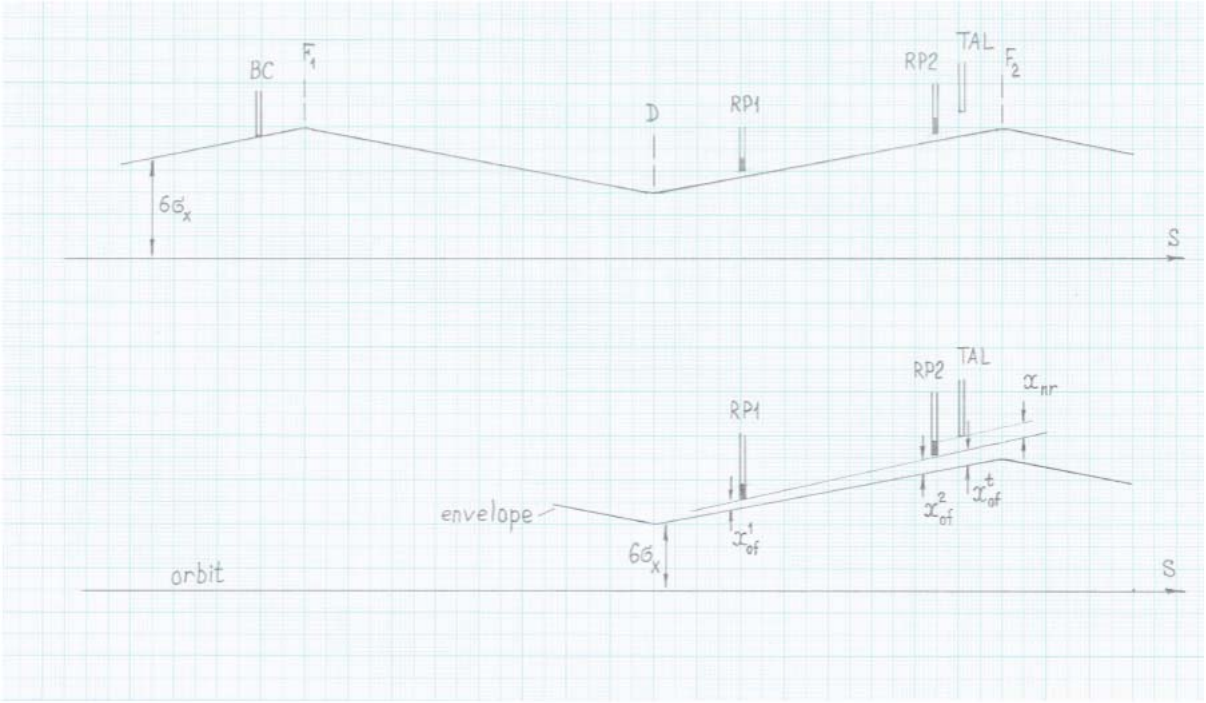

Figure 3: Conceptual scenario of the CRYSTAL experiment.

7. Simulation results for a 2-stage collimation without detectors

When 120-GeV protons cross the (111) Si channels of the 1 mm long crystal, bent by the angle α=150 μrad, the critical channeling angle is θ_c=20.4 μrad, the volume reflection (VR) angle is θ_{vr}=22 μrad and the RMS multiple scattering angle is θ_{ms}=10 μrad.

The nature of particle interaction with the crystal depends on the crossing angle θ of the incoming particles with the crystal planes. When $\theta<-\theta_c$ only multiple scattering occurs, producing random deflecting angles in all directions. When $|\theta|<\theta_c$ the particles are coherently deflected by the bend angle α. Finally when $\theta_c<\theta<\alpha$, the particles are coherently deflected by the VR angle θ_{vr} in the opposite side respect to crystal bending (negative deflection). This is true for an absolute value of θ smaller than α. Beyond this threshold, for $\theta>\alpha$, multiple scattering interactions occur again.

In the nominal position, the offset of the TAL edge from the $6\sigma_{beam}$ envelope is $\tilde{x}_{of}(TAL) = 1.66\,\mathrm{mm}$. To deflect halo particles into the TAL, the crystal should produce an angular kick of at least θ^*=51 μrad. In these conditions, only channeled particles, which are deflected by α=150 μrad, can reach the collimator. Particles deflected by multiple scattering or by VR will stay clear from the TAL and will repeatedly cross the crystal with a consequent diffusion-like increase of their emittance and a continuous betatron phase mixing at each crystal traversal. The diffusion rate due to VR is about twice larger than that due to multiple scattering. However, when the VR area is located at the edges of crystal, i.e. when the crystal is entirely oriented in one side respect to the beam envelope, the VR interaction can only produce an increase the betatron oscillation amplitude. In this case, the oscillation amplitude increases monotonously (and no longer in diffusive mode), producing a much faster drift of

the particle towards the collimator position. This fact leads to some peculiar features of the collimation efficiency as a function of the crystal orientation θ_0.

The crystal alignment is optimal for channeling when the crystal orientation angle is θ_o=0, i.e. when the crystal planes are parallel to the beam. In computer simulations we considered crystal alignments in a wide range of values around the optimum and evaluated the distribution of the impact parameter of the particles intercepting the TAL. Hereafter we give a selection of our results.

In Figure 4 we consider cases with θ_o=0 (row a), θ_o =20 μrad (row b), θ_o =40 μrad (row c) and θ_o =–20 μrad (raw d) and we give distributions of the impact parameter (left column), of the number of crystal traversals (central column) and of the number of turns performed before the hit with the TAL. In the plots of the left column, the abscissa x=0 corresponds to the transverse position of the edge of the TAL $x(TAL) = 6\sigma_{beam} + \tilde{x}_{of}(TAL) = 8.75\ mm$.

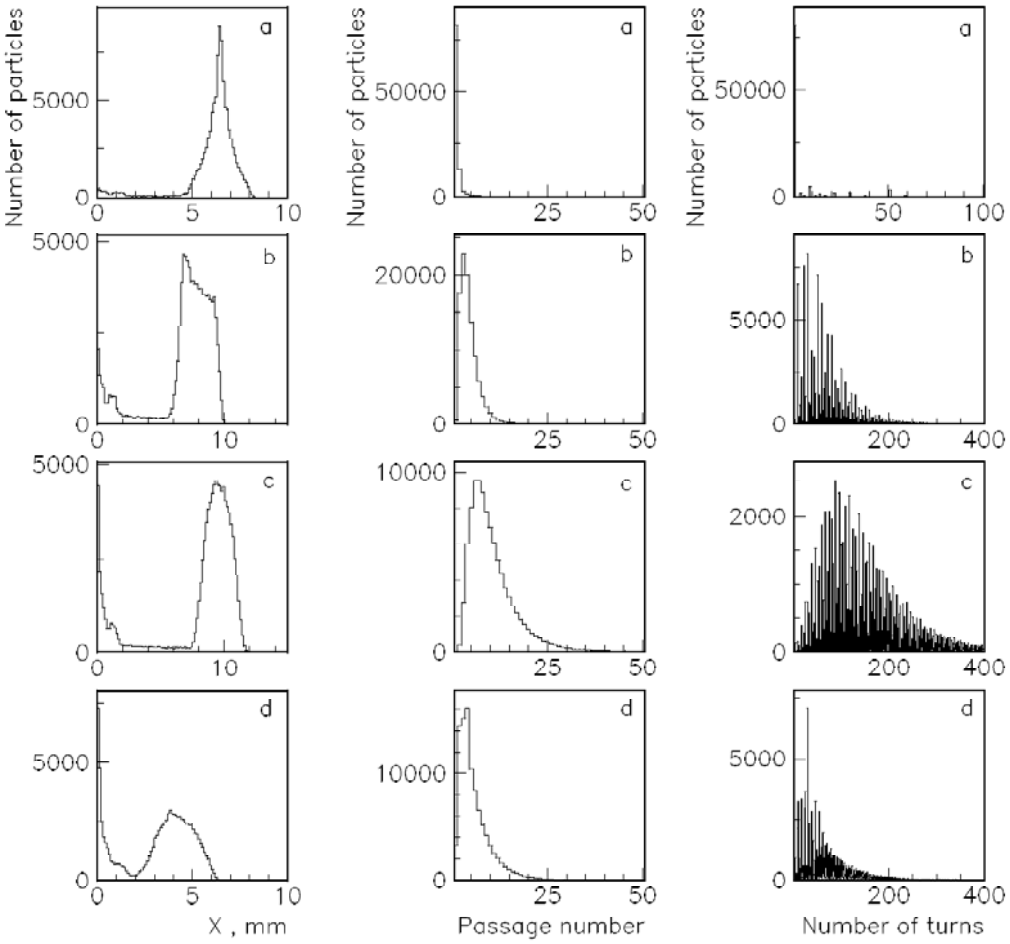

Figure 4: Distribution of the impact parameter (left), of the number of crystal traversal (centre) and of the number of turns (right) before the TAL hit with θ_o=0 (a), θ_o=20 μrad (b), θ_o=40 μrad (c) and θ_o=–20 μrad (d). The TAL edge is at x=0 (left).

For θ_o=0, the mean value of the impact parameter is larger than 6 mm (see Fig.4 left). It increases for positive values of θ_o because the crystal inclination adds up to the channeling kick. The peak at large x-values contains more than 80% of the particles, even for imperfect alignment at θ_o=40 μrad≈2θ_c (see Fig.4 case c, left). For θ_o=0, more than 80% of particles hit the collimator after the first crystal traversal (see Fig.4 case a, centre). By increasing θ_o the number of passages required to hit the TAL increases (see Fig.4 cases b, c and d, centre).

In Figure 5 we consider crystal orientations, which do not allow channeling and we show the distribution of impact parameter and of the number of crystal traversal before hitting the TAL. For θ_o=75 μrad (case a) we only have multiple scattering. For θ_o=-75 μrad (case b) we are in the middle of the VR angular range. For θ_o=-(α+θ*)=-251 μrad (case c), we have a case of special class, in which $\theta_o \leq -(\alpha+\theta^*)$. The crystal inclination is such that, initially, there is only multiple scattering and emittance diffusion, until when the particle inclination eventually reach the edge of the VR angular range. At this point, the emittance growth becomes a constant drift, instead of a diffusion, which brings faster the particles into the TAL.

In cases a and b, the impact parameter distribution has a sharp maximum at x=0 (see Fig.5 left). The distribution is wider in case b because of the larger deflection angle in VR regime. This also explains the smaller number of crystal traversal required in case b. In case c, the peak of the x-distribution is determined by the amplitude drift regime due to VR, by which the particles are deflected towards the TAL. The peack value is of about the same of the drift step-size induced by a single VR interaction, i.e. $x \approx \Delta x_m(\theta_{vr}) \approx 1.4$ mm.

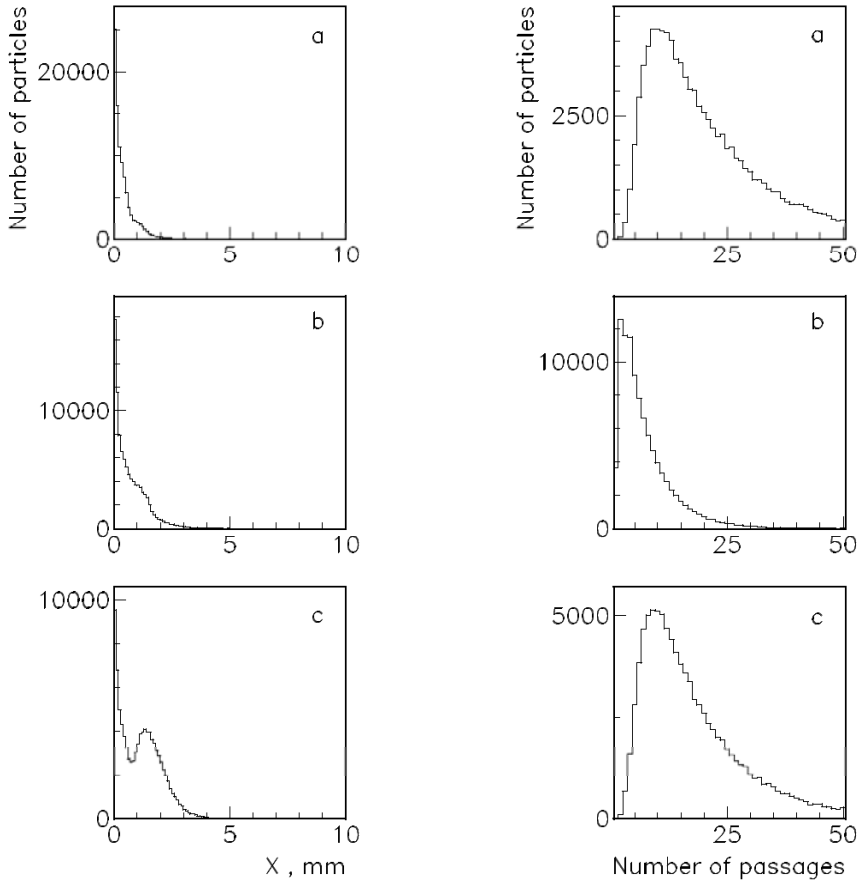

Figure 5: Distribution of the impact parameter (left) and of the number of crystal traversal (right) before the TAL hit with θ_o=75 μrad (a), =θ_o-75 μrad (b) and θ_o=-251 μrad (c). The TAL edge is at X=0 (left).

We are interested to evaluate the collimation efficiency, which is the ratio of the number of particles lost in the TAL by the number of particles hitting the crystal. Since in our SPS model the aperture restrictions are only the crystal and the TAL, the collimation inefficiency occurs only because of inelastic nuclear interactions in the crystal itself. Figure 6 shows the collimation efficiency as a function of the crystal orientation. The maximum near θ_0=0 is due

to channeling. The dashed line in the bottom is the efficiency in multiple scattering regime, plotted for comparison over the whole angular range.

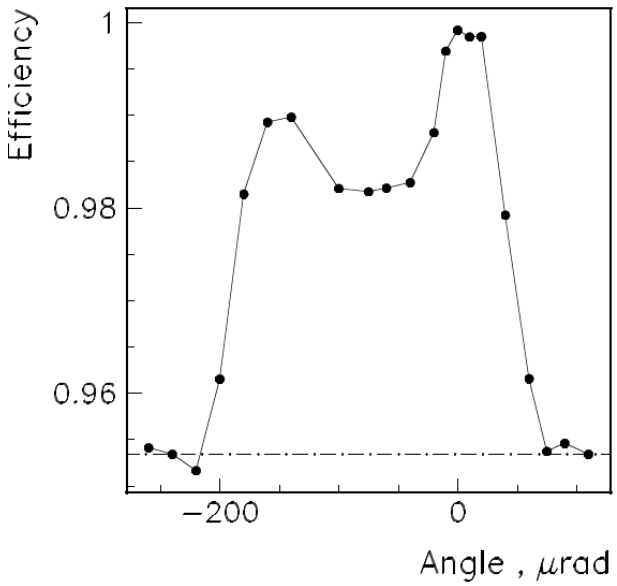

Figure 6: Collimation efficiency as a function of the crystal orientation.

Figure 7 shows the fraction of particles lost by inelastic interactions in the crystal as a function of the crystal orientation. For a given angle, the fraction of inelastic loss is the complement to one of the collimation efficiency. In VR regime the fraction of inelastic loss is smaller than in multiple scatering regime (see Fig.7 in the range -20 μrad≤θ_0≤-130 μrad). This is due to the larger VR angular deflection, which reduces the number of crystal traversal required to hit the collimator. A second minimum of inelastic loss appears at the orientation with $\theta_0 \approx -\alpha$=-150 μrad, when the whole VR angular range is entirely in the same side respect to the beam envelope inclination. As already mentioned, this minimum is due to the fast drift of the betatron oscillation amplitude, which decreases the number of crystal traversal.

Figure 8 shows the average value of the impact parameter as a function of the crystal orientation.The distribution has a maximum of 8 mm near $\theta_o \approx 2\theta_c$ due to channeling, the width of which is 70 μrad at the pedestal that is larger than $3\theta_c$. On the left, there is a flatish plateau of 0.75 mm due to VR, ending with a smaller peak of 1.25 mm heigth at 200 μrad, due to VR in drift regime. In multiple scattering the mean impact parameter is of 0.4 mm (dashed line in Fig 8).

Figure 9 shows the halo fraction, which hit the collimator near the edge, as a function of the crystal orientation. We computed that franction using two ranges of the impact parameter values one with x<0.5 mm (Fig.9, curve 1) and the other with x<1 mm (Fig.9, curve 2). The dashed lines are the corresponding values for multiple scattering. The dip at θ_o=0 is due to channeling and the dip at θ_o=200 μrad is due to VR in drift regime.

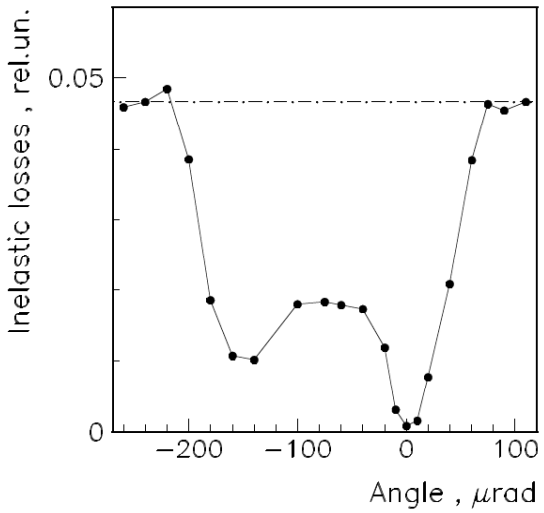

Figure 7: Fraction of inelastic particle loss as a function of the crystal orientation.

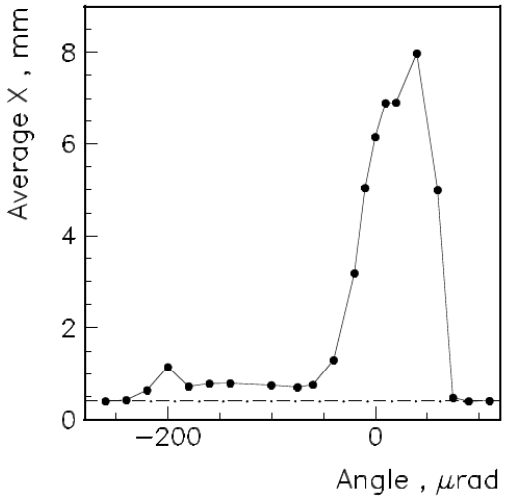

Figure 8: Average value of the impact as a function of the crystal orientation.

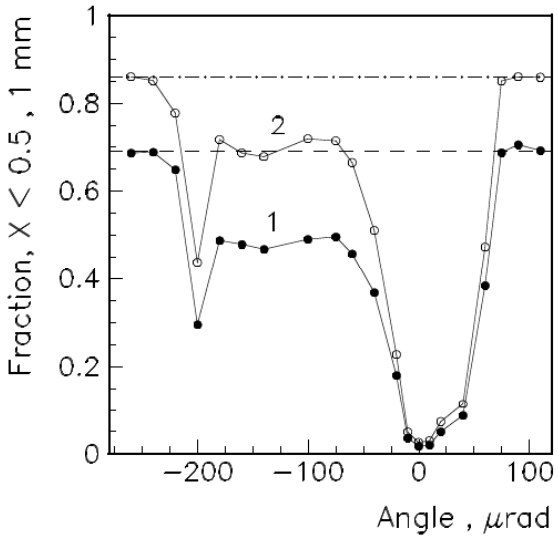

Figure 9: Halo fraction with impact parameter 0<*x*<0.5 mm (1) or 0<*x*<1 mm (2) as a function of crytal orientation.

8. Simulation results for a 2-stage collimation with detectors

To detect particle trajectories intercepting the TAL we use two roman pots, RP1 and RP2, with Si detectors (see Fig.3). As already mentioned, the RP1 is in a location with a small value of β_x particularly unfavorable to measure horizontal distances. Nonetheless, the coordinate and angular distributions of the incoming particles are still acceptable. In Figure 10, we show them for the crystal orientation value θ_o=0. The impact parameter has a peak at more than 4 mm from the RP1 edge, which in the plot is at x=0 (the RP1 edge has the offset x_{of}(RP1)=1 mm).

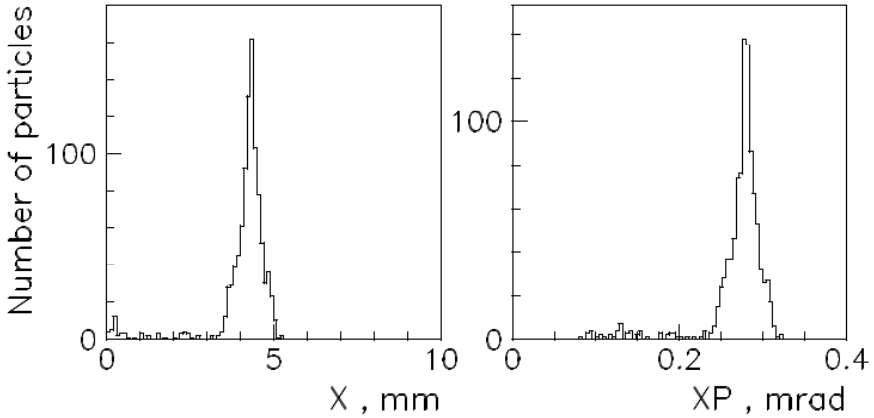

Figure 10: Distribution of the impact parameter (left) and of the deflection angle (right) at the RP1 with θ_o=0. The RP1 edge is at x=0 (left).

In traversing the roman pots, the incoming particles experience additional multiple scattering interactions, which induce as a detrimental side effect the broadening of the impact parameter and of the deflection angle distributions. Figure 11 shows them for crystal orientations, in which θ_o=0 (a), θ_o=20 (b), θ_o=-200 (c) and θ_o=75 μrad (d). In case c, the distributions are broadened and the VR maximum generated at $\theta_o \approx -(\alpha+\theta^*)$ is smoothed down.

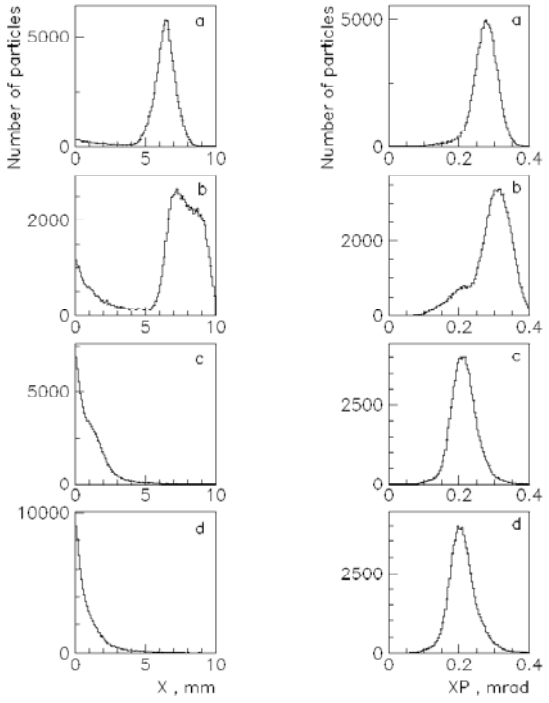

Figure 11: Impact parameter and angle for θ_o=0 (a), =20 (b), =-200 (c) and =75 μrad (d).

Figure 12 shows the collimation efficiency P_c as a function of the crystal orientation. In the same Figure, we also plot the halo fraction P_{r2}, which cross the sensitive area of the detector in RP2 and the fraction P_{r12}, which cross the active areas of the detectors in RP1 and RP2. In fact, P_{r2} is the probability to measure the impact parameter at the TAL and P_{r12} the probability to detect the angle of the incoming particle. Both P_{r2} and P_{r12} are close to 1 for angles near θ_o=0. For the crystal orientations, for which a large number of crystal traversal will occur, the probability to detect angles decreases sharply. The dashed lines refer to multiple scattering regime. Note that, by removing RP1 from the beam aperture, we can make $P_c \approx P_{r2}$.

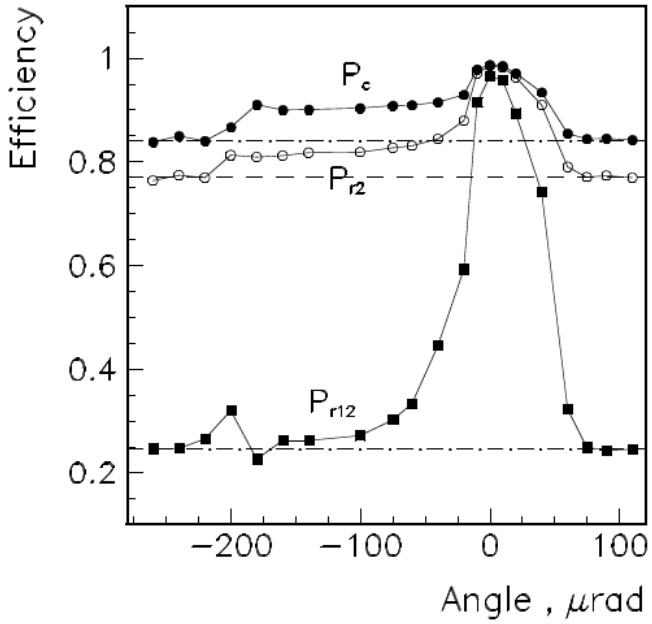

Figure 12: Collimation efficiency as a function of the crystal orientation. P_{r2} is the probability to detect impact parameters and P_{r12} the probability to detect the angles.

In Figure 13 we plot the inelastic loss fraction as a function of the crystal orientation. The plot in the left refers to inelastic interactions in the detectors and the plot in the right to loss in the cristal. The dashed lines refer to multiple scattering regime.

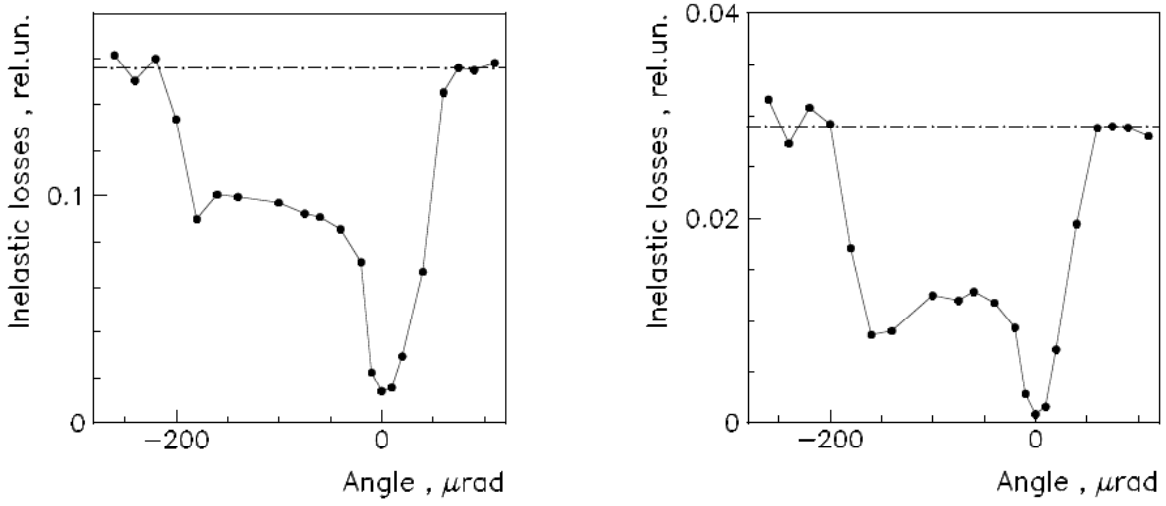

Figure 13: Inelastic loss fraction in the detectors (left) and in the crystal (right) as a function of the crystal orientation.

Figure 14 shows the average impact parameter with the collimator x_R as a function of the crystal orientation. The distribution has a peak of 6.5 mm about 100 μrad wide at the pedestal. The dashed line refers to multiple scattering regime.

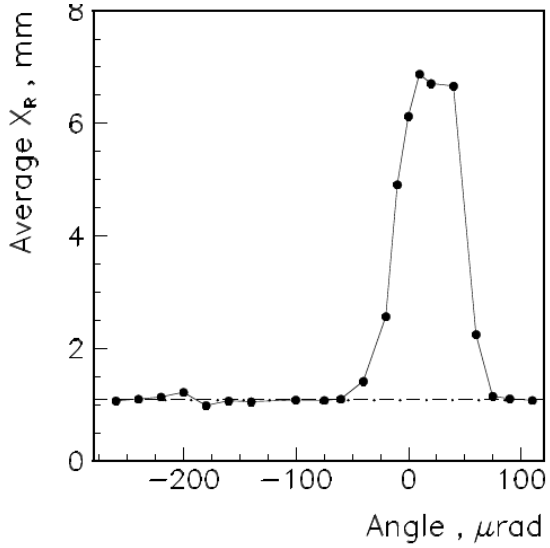

Figure 14: Average impact parameter x_R as a function of the crystal orientation.

Figure 15 shows the halo fractions, which hit the collimator, as a function of the crystal orientation. The impact parameter is in the range x<0.5 mm (Fig.15, curve 1) or x<1 mm (Fig.15, curve 2). The dip at θ_o=0 is due to channeling and the dip at θ_o=200 μrad is due to VR in drift regime. The dashed lines are the corresponding values for multiple scattering.

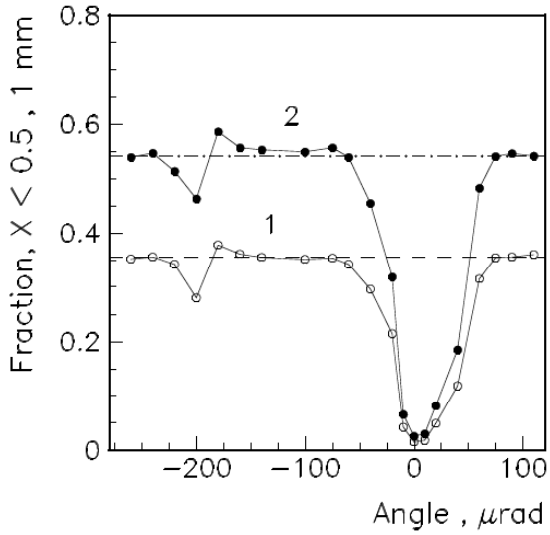

Figure 15: halo fraction with impact parameter 0<x<0.5 mm (1) or 0<x<1 mm (2) as a function of crytal orientation.

The simulation has been performed with a point-like beam dimension in the in (y,y′) phase space. Due to multiple scattering interactions in the crystal and in the roman pots, the beam has finite vertical dimension when intercepting the TAL. Examples of the vertical distribution of the TAL impact parameter are shown in Figure 16. The solid line refers to the crystal orientation with θ_o=-75 μrad and the dashed line to θ_o=60 μrad. For all crystal orientations, the distribution width at the pedestal is always smaller than 4 mm. The vertical beam diameter at 3σ is of about 3 mm. By linearly composing it with the vertical full-spread

induced by multiple scattering, the full size of the beam halo, which hit the crystal, is of about 7 mm. This is the minimal size of the crystal to avoid additional multiple scattering interactions at the crystal support, which may induce unwanted beam loss.

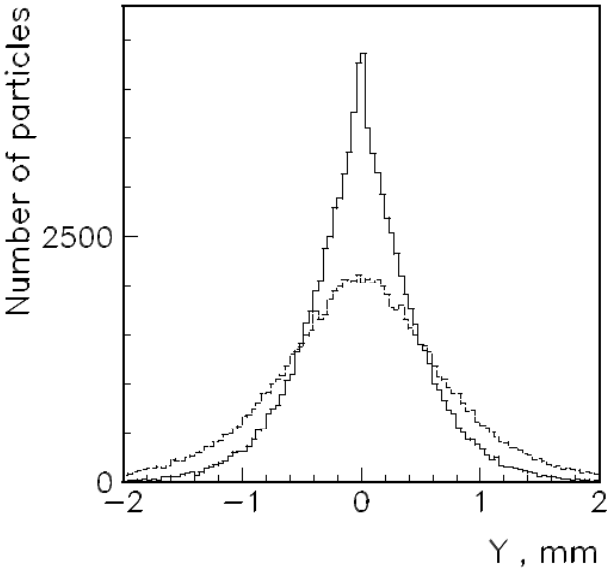

Figure 16: Distribution of the vertical impact parameter in the TAL for the crystal orientation with θ_o=-75 μrad (solid line) and with θ_o=60 μrad (dashed line).

9. Conclusions

We discussed the features of the experimental layout for the SPS crystal collimation experiment and we suggested optimal transverse positions of the crystal, detectors and collimator.

Using computer simulations, we checked that the experiment setup is appropriate and that the collimation efficiency is large in all conditions. We also observed that inefficiency results from inelastic nuclear interactions with the crystal and the detectors. Crystal collimation should have optimal performance in channeling mode, with most of the beam halo extracted in the first crystal encounter. Volume reflection regime is less efficient because of the smaller deflection angle and of the increased number of crystal encounter to extract the halo.

The roman pots have a rather perturbative effect on the beam dimension due to the increased probability of multiple scattering. This will result in a decrease of the collimation efficiency and of the average impact parameter at the collimator.

In absence of horizontal-vertical coupling, the vertical beam size has no effect on the efficiency.

We conclude that the experimental layout is fully adequate for our needs .

10. Acknowledgements

Many people contributed to define the CRYSTAL layout in CERN, INFN, PNPI, and IHEP. We would like to thank all them. We also would like to acknowledge the pioneering work of the H8RD22 collaboration in investigated the crystal-proton interactions in the range of energy of several GeV. S. Hasan prepared Figure 2.

We finally acknowledge the support of the European Community-Research Infrastructure Activity under the FP6 “Structuring the European Research Area” programme (CARE, contract number RII3-CT-2003-506395).

References

[1] M. Prest, W. Scandale, “The proposal of the CRYSTAL experiment”, CERN-SPSC 2008-0014, SPSC-P-335, Geneva, April 2008.

[2] W. Scandale et al., Phys.Rev.Lett. 98 154801(2007).

[3] B. N. Jensen et al. “A proposal to test beam extraction by crystal channeling at the SOSL a first step towards a LHC extracted beam”, CERN/DRDC 91-25, DRDC/P29, Geneva, July 1991.

[4] P. Strolin, CERN 69-6, Geneva, March 1969.

[5] E. Deile et al. “Tests of a roman pot prototype for the TOTEM experiment”, Proceedings of PAC05, Knoxville, Tenessee, USA, May 2005.